New Journal of Physics
The open access journal at the forefront of physics

Deutsche Physikalische Gesellschaft DPG
IOP Institute of Physics

Published in partnership with: Deutsche Physikalische Gesellschaft and the Institute of Physics

OPEN ACCESS

RECEIVED
26 April 2021

REVISED
19 August 2021

ACCEPTED FOR PUBLICATION
24 August 2021

PUBLISHED
10 September 2021

PAPER

Elastic and inelastic particles scattering by dust acoustic soliton. A new oscillatory process in dusty plasma

F M Trukhachev[1,2,3,*], N V Gerasimenko[3], M M Vasiliev[1,2] and O F Petrov[1,2]

[1] Joint Institute for High Temperatures of the Russian Academy of Sciences, Moscow, 125412, Russia
[2] Moscow Institute of Physics and Technology, Dolgoprudnyi, Moscow Region, 141701, Russia
[3] Belarusian-Russian University, Mogilev 212000, Belarus
[*] Author to whom any correspondence should be addressed.

E-mail: ftru@mail.ru

Keywords: soliton, particle scattering, wave–particle interaction, charged particles oscillation

Supplementary material for this article is available online

Abstract

The parameters of scattering (reflection) of charged particles by the leading edge of a dust acoustic soliton are analyzed. The soliton profile is calculated using the Sagdeev pseudopotential approach. To analyze the motion of charged particles, the Newton's second law is used. It is shown theoretically that the charged particle scattering can be elastic and inelastic. The nature of scattering significantly depends on the presence of dissipation. In the dissipative case, charged particles scattering is the process of an oscillatory nature. It is shown that it can be considered as a new type of oscillations of charged particles in plasma. The parameters of the oscillations are calculated both numerically (nonlinear case) and analytically (within the linear approximation). Theoretical results are compared with known experimental results, as well as the applied aspect is stated.

1. Introduction

Applications of plasma waves physics include: plasma heating in fusion devices [1], charged particle acceleration [2, 3], astrophysics [4], etc. The studying of a wave–particle interaction is the important component of this research area. Landau damping [5] and beam instabilities [6, 7] are examples of the linear wave–particle energy exchange processes. These phenomena affect the particle distributions and can be analyzed within the framework of the wave kinetic theory. Nonlinear effects appear in the case of large amplitude waves, namely: (1) the formation of the electron phase-space hole caused by the resonance trough trapping of particles [8–10]; (2) unidirectional transfer of charged particles by an electric field of solitons and the excitation of soliton currents [11–13]; (3) generation of accelerated particle beams and formation of multi-streaming flows by nonlinear waves and solitons of supercritical amplitude [14–16].

Let us consider the last case in more detail. Nonlinear electron oscillations of large amplitude were studied theoretically in [17]. Plane oscillations in homogeneous plasma were found to be stable below critical amplitude. For larger amplitudes it was found that multi-streaming flow develops on the first supercritical oscillation. Subcritical amplitudes are characterized by the resonant motion of electrons in the oscillatory field. The amplitude threshold for the wave breaking is significantly reduced in warm plasmas [18]. The phenomenon of the breaking of powerful electron plasma waves was also observed experimentally [19]. It is important to note that the speed of electrons accelerated by the wave was twice the speed of the wave itself in the case of a collisionless plasma. The process of breaking of strongly nonlinear waves and solitons in collisional plasmas was studied in experiments [14–16]. The speed of particles accelerated by the wave in the collisional case was equal to the wave speed. Particles in this case seemed to 'stick' to the leading edge of the wave. In [15] this process is called 'no-trough trapping', because the traditional potential well [12] in the case [14–16] was not observed. According to [15, 16], the phenomenon of sticking accelerated

particles to the front of the wave is caused by dissipative forces. It was also presented in [16] that in the collisional case, particles experience large-amplitude oscillations before sticking to the front of the wave.

In this work, it is shown that the oscillations described in [16] can be considered as a new oscillatory process in plasma. A more rigorous model of warm plasmas is proposed, within the framework of which subcritical solitons are able to scatter particles of the Maxwellian tail. We will assume that there are not many such particles and their influence on the soliton can be neglected in the first approximation. An analysis of the new oscillations is carried out. The collisionless and collisional cases are considered within the paradigm of elastic and inelastic scattering of particles by solitons and nonlinear waves. The theoretical results obtained in the work are compared with known experiments.

2. Theoretical model

Let us consider a dust acoustic (DA) mode for analyzing the process of scattering of charged particles by a soliton. The main reason for this choice is the availability of detailed experimental data, presented in [14–16]. Experiments in the dusty plasma provide unique opportunities for analyzing both the evolution of waves [20, 21] and the motion parameters of individual charged particles interacting with the wave [14–16, 22, 23].

Results obtained for the DA mode can be easily generalized to the cases of ion- and electron-acoustic modes due to their similarity.

Interacting dust charged particles can be divided into two groups. The first group includes transit particles that remain inside the soliton profile for a short time. All kinematic parameters of the transit particles in front of the conservative soliton and behind it are the same, except for the position in space, which changes by several Debye radii [11, 13]. Such particles do not decrease the energy of the conservative soliton, so the process can be considered as adiabatic. The properties of the transit particles in the dissipative case are considered in detail in [24], where the difference between dissipative and conservative solitons was discussed. The second group includes scattered particles that are accelerated by the soliton to velocity V_p, which is exceeding soliton velocity V_{sol} or equal to it ($V_p \geqslant V_{sol}$). In this case one can observe a multi-streaming flow of charged particles. It is shown in [16] that $V_p \approx V_{sol}$ in the presence of dissipation and $V_p = 2V_{sol}$ in the collisionless case. The acceleration of particles of the second group is provided by the energy of the soliton, this process leads to the damping of the wave. It is worth noting that in open systems, nonlinear waves and solitons can receive energy from external energy sources [25, 26] such as beams of charged particles, external electric fields, etc. In this case, self-excitation of waves can be observed with an evolution of a different nature, such as amplification, steepening, stationary propagation, breaking.

We consider a stationary wave process, where amplification and dissipation processes are in balance. Let us focus in more detail on the analysis of the scattered particles properties. In the case of electron waves, they are registered by grid analyzers [19], in the case of DA waves, their properties are measured directly by using high-frequency video cameras [14–16]. If there are many particles of such type, this inevitably affects both nonlinear waves and a medium. In particular, the breaking of nonlinear waves and solitons is observed in [14, 16, 19], which leads to the formation of cavitons (local decrease in plasma concentration) [19] and the plasma heating [14, 15]. In the case of warm plasmas the acceleration (scattering) begins with particles of the Maxwellian tail.

Let us consider the case of a warm dusty plasma. We assume that the plasma contains populations of electrons, ions, monodisperse negatively charged dust particles, and a neutral gas. We do not take into account the influence of external electric and magnetic fields. Then, for the DA mode, we can write the following condition [27].

$$V_{sol} \sim C_d \ll V_{Ti} \ll V_{Te}, \tag{1}$$

where C_d is DA velocity, $\upsilon_{Te,Ti} = \sqrt{T_{e,i}/m_{e,i}}$ is thermal velocities of electrons and ions. Figure 1 schematically shows the soliton–particle interaction in the wave frame. In this frame all particles drift from right to left with a velocity V_{sol} everywhere except the soliton location region. In accordance with inequality (1), the drift of ions and electrons can be neglected, considering their distribution to be Boltzmann, but for dust particles, the drift cannot be neglected. In figure 1, trajectories of the transit particles are shown by the solid curve, trajectories of the scattered particles by the dashed curve. In our chosen frame the problem can be reduced to the scattering of the dust particles by the static soliton. In the Lagrange form, the particle motion can be described by the following equation:

$$m_d \frac{d^2\xi'}{dt^2} = F_{sol} - \nu_{dn}\left(\frac{d\xi'}{dt} - V_{sol}\right), \tag{2}$$

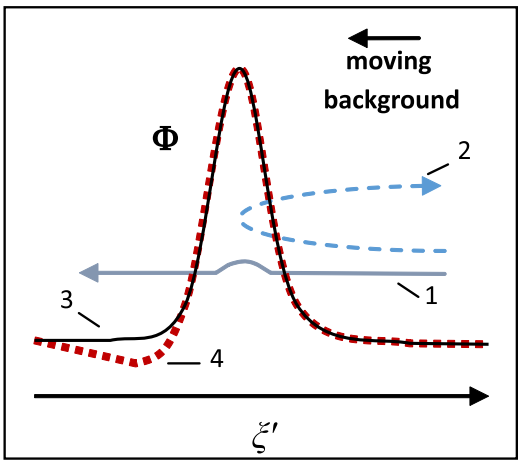

Figure 1. Schematic representation of the soliton-particle interaction in the moving (wave) frame; curve 1 - transit particles, curve 2 - scattered (reflected) particles, 3 - classical soliton profile, 4 - damped soliton profile (see details in[29]).

where $\xi' = x - V_{\rm sol} \cdot t$. Hereinafter, the symbols ξ, ξ' denote the coordinate of the particle in the wave frame, while the symbols x, X are used for the fixed frame. $F_{\rm sol}$ is the electric force acting on the dust particle from the soliton. This force is localized in space. The dissipative force is described by the second term on the right-hand side of equation (2), where $\nu_{\rm dn}$ is dust-neutral collision frequency which expressed by the formula $\nu_{\rm dn} = 8\sqrt{2\pi} r_{\rm d}^2 n_{\rm n} T_{\rm n} / (3 m_{\rm d} \upsilon_{\rm Tn})$ [28], where $r_{\rm d} = {\rm const.}$ is a dust particle radius, $\upsilon_{\rm Tn} = \sqrt{T_{\rm n}/m_{\rm n}}$ is a thermal velocity of neutral gas atoms (molecules). We consider the neutral drag force as the only dissipation mechanism. Equation (2) is similar to equation (7) from [16], but here the wave frame is used. Therefore, the dissipative term is written taking into account the drift of the neutral gas with a velocity of $-V_{\rm sol}$.

To solve equation (2), it is necessary to specify a soliton profile, which allows to determine the force $F_{\rm sol}$. To date no self-consistent models describing stationary dissipative acoustic solitons were presented. Nevertheless, a number of important physical phenomena can be described by using the classical soliton profile. As we show below, this approach is verified experimentally. Section 4 discusses the results of experiments in collisional plasmas, in which nonlinear waves have a soliton-like profile. The reasonableness of using the classical profile to describe the properties of dissipative solitons is confirmed by theoretical models [29, 30]. These models are not stationary, since they take into account only the dissipation, but do not consider external amplification forces. Evolution in this case corresponds to slow decay. It was also shown that for small dissipation, the profile of the dissipative soliton is close to the classical ($\sim {\rm sech}^2(x)$). A more rigorous numerical solution of the KdV equation (see [29]) gives the profile shown in figure 1 by the dotted curve. In work [16], where the oscillations under study were discovered for the first time, the calculations were carried out under the assumption of the classical soliton profile. This approach is not self-consistent, although it gives a satisfactory description of experimental results. We use the same approach, but take into account the pressure of the dust component associated with the thermal motion of dust particles. The system of normalized hydrodynamic equations can be written in the form [31, 32]:

$$N_{\rm e}(\Phi) = \exp\left(\frac{e\varphi}{T_{\rm e}}\right) \equiv \exp(\sigma_{\rm i}\Phi), \tag{3}$$

$$N_{\rm i}(\Phi) = \exp\left(-\frac{e\varphi}{T_{\rm i}}\right) \equiv \exp(-\Phi), \tag{4}$$

$$\frac{\partial \upsilon_{\rm d}}{\partial \tau} + \upsilon_{\rm d}\frac{\partial \upsilon_{\rm d}}{\partial X} = \frac{\partial \Phi}{\partial X} - \frac{\sigma_{\rm d}}{N_{\rm d}}\frac{\partial P_{\rm d}}{\partial X}, \tag{5}$$

$$\frac{\partial P_{\rm d}}{\partial \tau} + \upsilon_{\rm d}\frac{\partial P_{\rm d}}{\partial X} + 3P_{\rm d}\frac{\partial \upsilon_{\rm d}}{\partial X} = 0, \tag{6}$$

$$\frac{\partial N_{\rm d}}{\partial \tau} + \frac{\partial N_{\rm d}\upsilon_{\rm d}}{\partial X} = 0, \tag{7}$$

$$\frac{\partial^2 \Phi}{\partial X^2} = \delta_{\rm e}N_{\rm e} - \delta_{\rm i}N_{\rm i} + N_{\rm d}. \tag{8}$$

Here densities, initial densities, and normalized densities of particles are denoted as n_j, n_{0j}, $N_j = n_j/n_{0j}$, respectively, where $j = ({\rm e; i; d; n})$ corresponds to electrons, ions, dust particles and neutral atoms (molecules); φ and $\Phi = e\varphi/T_{\rm i}$ are potential and normalized potential respectively; Z is dimensionless dust

charge; $C_d = \sqrt{ZT_i/m_d}$ is the DA velocity; $\delta_j = n_{0j}/(Zn_{0d})$ (quasi-neutrality condition gives $\delta_e - \delta_i + 1 = 0$); P_d is the dust fluid pressure normalized by $p_0 = n_{0d}T_d$; $\sigma_i = T_i/T_e$ and $\sigma_d = T_d/(Z \cdot T_i)$; υ_d is dust velocity normalized by C_d; $X = x/\lambda_D$, $\tau = t\varpi_d$ where $\lambda_D = \sqrt{T_i/4\pi Zn_{0d}e^2}$ is a Debye radius, $\omega_d = \sqrt{4\pi n_{0d}Z^2e^2/m_d}$ is a plasma frequency for the dust component.

In the general case, the dissipative and amplifying mechanisms should be taken into account in equations (3)–(8) (see, for example, [33] for linear problem). Unfortunately, strongly nonlinear hydrodynamic self-consistent models for describing DA waves containing both dissipation and amplification do not yet exist. Therefore, we use the following approximation. In the stationary case, we consider the dissipative and amplifying forces to be small and compensating each other. A similar approach was used in works [16, 24].

Let us introduce the boundary conditions $\Phi, \upsilon_d \to 0$ and $N_j, P_d \to 1$ for $X \to \pm\infty$. We apply the following substitution $\xi = X - M\tau$, where $M = V_{sol}/C_d$ is the Mach number. This substitution reduces system (3)–(8) to the equation:

$$\frac{d^2\Phi}{d\xi^2} = -\frac{dE}{d\xi} = \delta_e \exp(\sigma_i\Phi) - \delta_i \exp(-\Phi) + N_d(\Phi), \tag{9}$$

where $E = -\partial\Phi/\partial\xi$ is the normalized electric field. The dust density can be expressed as:

$$N_d(\Phi) = \frac{\sigma_1}{\sqrt{2}\sigma_0}\sqrt{1 + \frac{2\Phi}{M^2\sigma_1^2} - \sqrt{\left(1 + \frac{2\Phi}{M^2\sigma_1^2}\right)^2 - 4\frac{\sigma_0^2}{\sigma_1^4}}}, \tag{10}$$

where $\sigma_0 = \sqrt{3\sigma_d/M^2}$, $\sigma_1 = \sqrt{1 + \sigma_0^2}$. A detailed derivation of the formulas (9) and (10) is presented in works [31, 32]. An expression for the Sagdeev pseudopotential $U(\Phi)$ can be written in the form $0.5\left(d\Phi/d\xi\right)^2 + U(\Phi) = 0$, where:

$$U(\Phi) = \frac{\delta_e}{\sigma_i}\left[1 - \exp(\sigma_i\Phi)\right] + \delta_i\left[1 - \exp(-\Phi)\right] - M^2\sqrt{\sigma_0}\left(\exp\left[\frac{\theta(\Phi)}{2}\right] + \frac{1}{3}\exp\left[-\frac{3\theta(\Phi)}{2}\right] - Y\right). \tag{11}$$

Here $\theta(\Phi) = \cosh\left[\frac{\sigma_1^2}{2\sigma_0}\left(1 + \frac{2\Phi}{M^2\sigma_1^2}\right)\right]^{-1}$, $Y = \exp\left[\frac{\theta(0)}{2}\right] + \frac{1}{3}\exp\left[-\frac{3\theta(0)}{2}\right]$. The constant Y is chosen so that the condition $U(0) = 0$ is satisfied. The normalized electric field is given by:

$$E(\Phi) = \pm\sqrt{-2U(\Phi)}. \tag{12}$$

For solitons of a small amplitude ($|\tilde{\Phi}| \ll 1$), equation (11) has approximate analytical soliton solutions, which is presented in [24, 32]. In our research we use numerical methods to solve equation (11) for arbitrary amplitudes.

As a basis we take the plasma parameters presented in [32]: $\sigma_i = 0.2$, $\sigma_d = 0.02$, $\delta = \delta_i/\delta_e = 10$. Figure 2 shows soliton profiles for different values of M. Reflected particles were not taken into account in warm plasma models [31, 32]. However, reflected particles must be present in warm plasma. Let us determine their properties using equation (2) for a probe particle, which takes the following form with the introduced normalizations:

$$\frac{d^2\xi}{d\tau^2} = \frac{\partial\Phi(\xi)}{\partial\xi} - \Omega\left(\frac{d\xi}{d\tau} + M\right). \tag{13}$$

Here $\Omega = \nu_{dn}/\omega_d$. Differential equation (13) can be integrated numerically (by Runge–Kutta method) using the previously found soliton profile $\Phi(\xi)$ (see figure 2).

We set the initial particle position to $\xi(0) = 25$, which is sufficient to prevent the soliton action on the particle at the initial moment of time. In the moving frame, particles hit the soliton from the right with an average speed of $(-M)$. Thus, the initial velocity of the particles will be set in the form $(-M + \Delta)$, where Δ is an additive, associated with the velocity distribution of particles. The introduction of the parameter Δ allows us to take into account the kinetic temperature of the dust component. Result of the integration of equation (13) is presented in figure 3(a). Figure 3 shows dependences $\xi(\tau)$ for particles at different values of Δ and Ω. The parameter $M = 1.19$ is close the critical value, in this case the soliton amplitude is close to the maximum. For clarity, the result is shown in the wave frame (figure 3(a)) and in the fixed frame (figure 3(b)). In the latter case, equation (13) takes the form [16]:

$$\frac{d^2X}{d\tau^2} = \frac{\partial\Phi(X)}{\partial X} - \Omega\left(\frac{dX}{d\tau}\right). \tag{14}$$

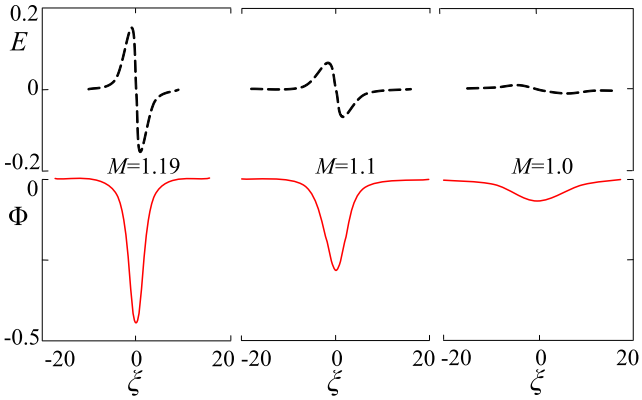

Figure 2. Profiles of the electric field $E = -\partial\Phi/\partial\xi$ (dashed curves) and the electric potential $\Phi(\xi)$ for the DA soliton at $\sigma_i = 0.2$, $\sigma_d = 0.02$, $\delta = 10$ for different values of M.

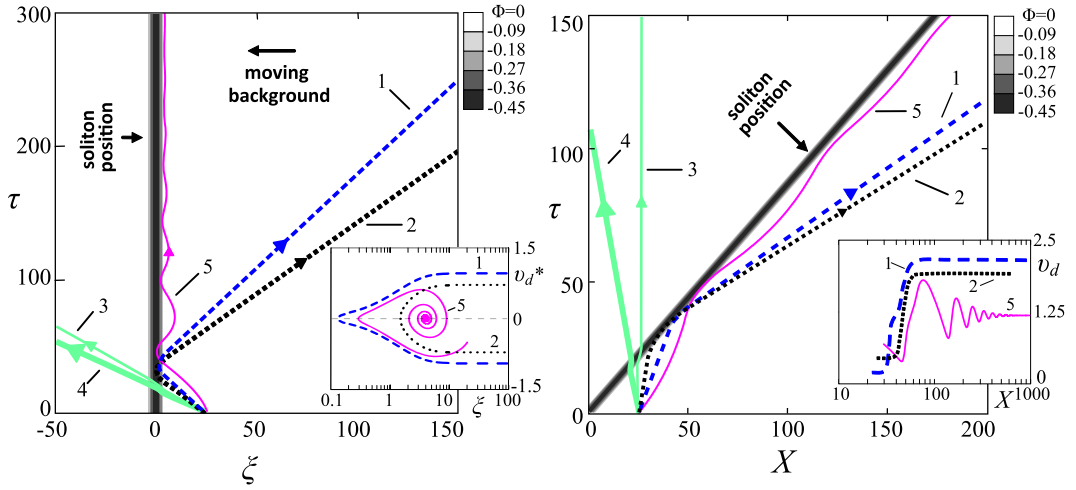

Figure 3. The parameters of motion of dust particles $\xi(\tau)$, $X(\tau)$ obtained from the numerical integration of equations (13) and (14) for moving (a) and fixed (b) frames, respectively. The parameters correspond to figure 2 at $M = 1.19$. The initial position of all particles is $X(0) = 25$. Parameters Δ and Ω are different for different curves: curve 1—$(\Delta, \Omega) = (0.25, 0)$; curve 2—$(\Delta, \Omega) = (0.48, 0)$; curve 3—$(\Delta, \Omega) = (0, 0)$; curve 4—$(\Delta, \Omega) = (-0.24, 0)$; curve 5—$(\Delta, \Omega) = (0.96, 0.03)$. Insert plots show dependences of velocities of reflected particles on the spatial coordinate (phase portraits).

Here we assume that $\frac{\partial\Phi}{\partial X} = \frac{\partial\Phi}{\partial\xi}$. Presented graphs are superimposed on the position of the soliton in space, the amplitude of which is shown by the contour plot. The dynamics of the wave–particle interaction is clearly shown in the simulation [34].

2.1. Elastic particles scattering ($\Omega = 0$)

Particles 1–4 in figure 3 (straight lines) correspond to the non-dissipative (conservative) case. Numbers 1, 2 correspond to reflected particles, while numbers 3, 4 describe transit ones. For particles 1–4, the dependences $X(\tau)$ and $\xi(\tau)$ are described by straight lines everywhere except the vicinity of the soliton. Let us introduce the notation for the normalized velocity of a dust particle: $v_d = dX/d\tau$ and $v_d^* = d\xi/d\tau$ in the fixed and wave frame, respectively. It is obvious that $v_d^* = v_d - M$. In the wave frame, velocity of the particle before and after interaction with the soliton is the same $|v_d^*(-\infty)| = |v_d^*(\infty)|$. This follows from the analysis of the inclination angles of curves 1–4 to the vertical axis. The nature of the reflection of particles 1, 2 fully corresponds to the process of elastic reflection (scattering). The equality $-v_d^*(-\infty) = v_d^*(-\infty)$ for reflected particles 1–2 is also shown in the inset to figure 3(a) and section 1.2 of [34]. This means that the velocities of reflected particles change sign from negative to positive, while velocities of passing particles remain negative. The equality $|v_d^*(-\infty)| = |v_d^*(\infty)|$ holds due to the conservative nature of the electric field produced by the soliton. Indeed, in a wave frame, the soliton field is stationary ($d\varphi/dt = 0$). The energy conservation law gives $Ze\varphi + \frac{m_d(v_d^*)^2}{2} = \text{const.}$, but the electric

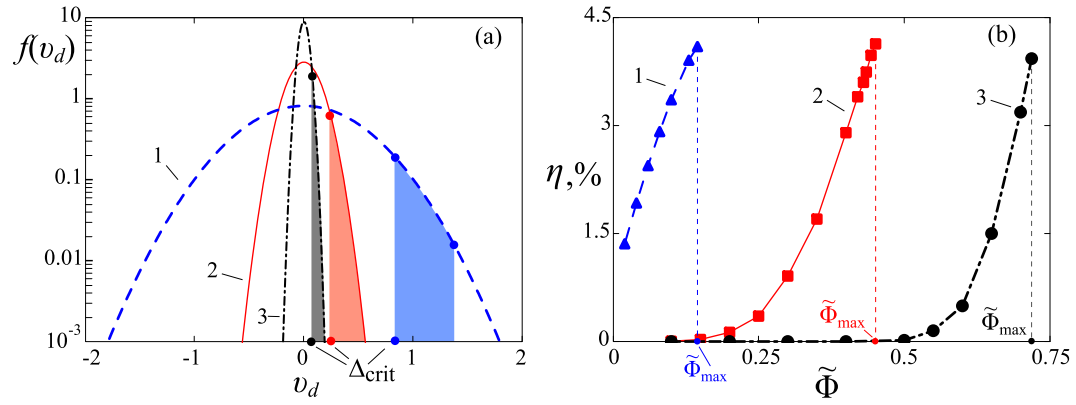

Figure 4. (a) Maxwell distribution functions for the dust fraction. The shaded areas correspond to particles that reflect by near-critical solitons ($\tilde{\Phi} \approx \tilde{\Phi}_{\max}$). (b) Dependencies $\eta(\tilde{\Phi})$. All parameters correspond to figure 2, except for the varied parameter σ_d: curves 1—$\sigma_d = 0.24$; curves 2—$\sigma_d = 0.02$; curves 3—$\sigma_d = 0.002$.

potential of the soliton is equal to zero everywhere except its vicinity and therefore $\frac{m_d (v_d^*)^2}{2} = \text{const}$. everywhere except the vicinity of the soliton.

Let us note here an interesting analogy between the phenomenon under study and the phenomenon of total internal reflection in optics. One can imagine that trajectories of particles are rays of light. In this case the potential of an electric field, produced by a soliton corresponds to the refractive index of a medium. Although this analogy is formal, perhaps it will help to formalize other properties of the process under study in the future.

In the fixed frame, the initial velocities of particles are close to zero. The deviation from zero is set by the Δ parameter and is determined by the Maxwell distribution. For subcritical solitons, most of particles are transit (see curves 3, 4 in figure 3). Reflection starts at $\Delta \geqslant \Delta_{cr} = 0.25$ for the considered set of soliton parameters. Only particles of the Maxwellian tail (curves 1, 2 in figure 3) are reflected by the soliton. The inset in figure 3(b) shows that initial speed $v_d(0) = \Delta$ corresponds to final speed $v_d(\infty) = 2M - \Delta$. For small values of Δ (i.e. $\Delta \ll M$) we have $v_d(\infty) \approx 2M$ (see also section 1.1 in [34]).

Let us estimate the number of reflected particles in the case of subcritical soliton. We can use $\eta(\Delta) = \int_{\Delta \cdot C_d}^{V_{sol}} f(v)\, dv$ formula, where $f(v) = \sqrt{\frac{m_d}{2\pi T_d}} \exp\left(-\frac{mv^2}{2T_d}\right)$ is the Maxwell–Boltzmann distribution function. By applying normalizations we get:

$$\eta(\Delta) = \int_{\Delta}^{M} f(v_d)\, dv_d, \tag{15}$$

where $f(v_d) = \frac{1}{\sqrt{2\pi\sigma_d}} \exp\left(-\frac{v_d^2}{2\sigma_d}\right)$. Equation (15) is written in the fixed frame for convenience. The velocity of the soliton is chosen as the upper limit of the integral, since particles with higher speeds do not reflect by the front of the soliton. Note that for $\sigma_d \ll 1$ the number of such particles is negligible, therefore, we can assume $+\infty$ as the upper limit of integral (15). We have $\eta_{cr} = \eta(\Delta_{cr}) = 0.037$ at $\Delta = \Delta_{cr} = 0.25$, where Δ_{cr} is the critical value of Δ for chosen parameters and $M = 1.19$, $\Omega = 0$. Particles are scattered if $\Delta \geqslant \Delta_{cr}$. Thus, approximately 4% of particles experience the elastic reflection. Presence of such particles leads to the formation of multi-streaming flow. Particles in this case are accelerated by the energy of the soliton. The MHD models used in [31, 32] neglect the influence of such particles.

Figure 4 shows dependences $f(v_d)$ and $\eta(\tilde{\Phi})$ for different values of σ_d. All other parameters correspond to figure 2. As it is shown in figure 4(a), with σ_d increase, the plot of $f(v_d)$ broadens, and one can expect an increase in the fraction of reflected particles. However, as it is shown in [31, 32], an increase in σ_d leads to a decrease in the soliton amplitude $\tilde{\Phi}$. Shaded areas in figure 4(a) correspond to reflected particles for solitons with large amplitudes close to the critical ones ($\tilde{\Phi} \approx \tilde{\Phi}_{\max}$). The critical amplitudes $\tilde{\Phi}_{\max}$ for different values of the parameter σ_d are shown in figure 4(b). It can be seen from figure 4(b) that the fraction of reflected particles η increases along with soliton amplitude $\tilde{\Phi}$ in a wide range of values of σ_d. In all considered cases, the maximum value of η does not exceed 5%.

The situation changes when the amplitude is supercritical [16]. For supercritical solitons, there are a lot of reflected particles ($\Delta_{cr} \sim 0$), which leads to its breaking. As shown above, the velocity of reflected particles in the fixed frame is equal to $v_d(\infty) = 2M - \Delta$. For $\Delta = 0$, we get $v_d(\infty) = 2M$. This means that in the case of elastic reflection of particles by a soliton (or a nonlinear wave) of supercritical amplitude,

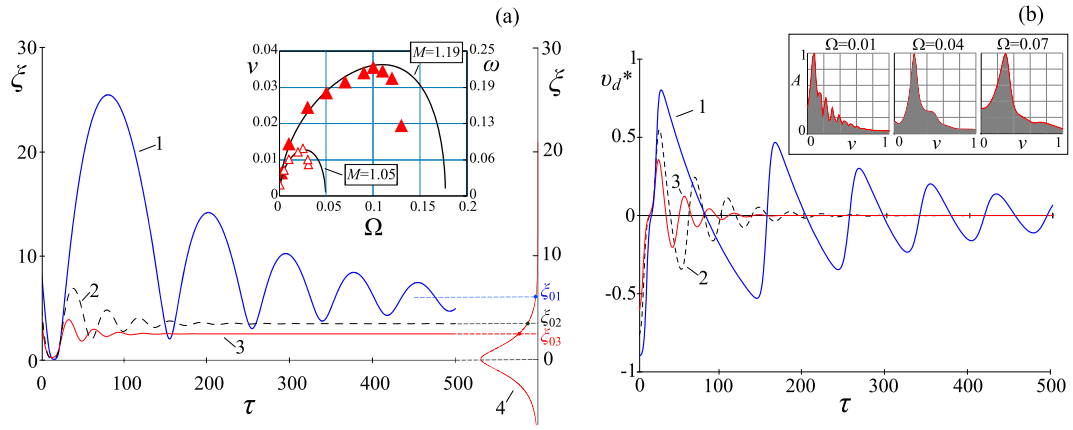

Figure 5. Time dependences of coordinates $\xi(\tau)$ (a) and velocities $\upsilon_{\rm d}^{*} = {\rm d}\xi/{\rm d}\tau$ (b) for dust particles in the wave frame at different values of Ω: curve 1—$\Omega = 0.01$; curve 2—$\Omega = 0.04$; curve 3—$\Omega = 0.07$. Curve 4 corresponds to the profile of the soliton $\Phi(\xi)$, the plot of which is aligned with the plot of $\xi(\tau)$. Plasma parameters correspond to figure 2 at $M = 1{:}19$. Equilibrium points $\xi_{01}, \xi_{02}, \xi_{03}$ are marked on the soliton profile. The insets show dependences $\nu(\Omega)$, $\omega(\Omega)$(left) and spectra (right). The dependence $\nu(\Omega)$ is plotted for different values of M. The solid curves are obtained analytically, while the exact numerical results are displayed by triangles.

the velocity of particles is equal to twice the soliton velocity. This result was obtained theoretically in [16] and some experiments [19] (see section 4). It is important to mention that if the soliton is supercritical, then the velocity of the reflected particles does not depend on either the soliton amplitude or the shape of its profile. This pattern is a consequence of the electrostatic nature of the soliton field.

2.2. Inelastic scattering ($\Omega \neq 0$)

In the non-dissipative case discussed above, elastically scattered particles quickly leave the vicinity of the soliton. In the presence of dissipation, the behavior of reflected particles changes significantly (we do not consider transit particles here). As can be seen from figure 3(a) and simulation [34] (section 2.2), in the wave frame the reflection process of particle '5' appears as damped oscillation. We can observe that reflected particles tend to 'stick' to the front of the soliton. This process is similar to the inelastic scattering, well known from mechanics. The steady-state velocity of such particles tends to the velocity of the soliton in the fixed frame [14–16, 34] (section 2.1) or to zero in the wave frame [34] (section 2.2). In the experimental work [15], this process was called *no-trough trapping*. It is caused by dissipative forces [15, 16]. It was shown in [32] that the negative potential of DA solitons is the potential well for positive ions, it is also the potential hump for negatively charged dust particles. Thus, the mechanism of trapping ions and dust particles is fundamentally different. Let us consider the trapping process in the wave frame. The friction force is given by $F_{\rm dis} = \Omega\left(\frac{{\rm d}X}{{\rm d}\tau} + M\right)$. In the undisturbed state, particles drift from right to left with velocity $\frac{{\rm d}X}{{\rm d}\tau} = -M$, so $F_{\rm dis} = 0$. Interaction with the soliton causes fluctuations of the particle velocity. In this case, a non-zero friction force arises $F_{\rm dis} \neq 0$, which tends to restore the initial value of the particle velocity. Thus, the soliton field tends to reflect the particle incident from the right, but the friction force accelerates the particle in the initial direction of motion (from right to left). In other words, the friction force tends to pull the particle against the soliton, which, in turn, repulses it. As a result, oscillations arise. Hence, the motion of the potential hump, and non-zero friction force are necessary conditions for particles trapping. The trapping mechanism is theoretically described in [15, 16] using different approaches. Oscillations that occur during the trapping process were first mentioned in [16] within the study of soliton breaking processes.

3. A new oscillatory process

3.1. Numerical modeling

Let us consider the main issue of our research, namely, the analysis of the properties of the new oscillatory process in plasma. Figure 5 shows dependences $\xi(\tau)$ and $\upsilon^{*}{}_{\rm d}(\tau)$ for different values of Ω. Figure 5 demonstrates that the oscillation amplitude decreases along with Ω. We denote oscillation frequency as ν. Dependence $\nu\,(\Omega)$ is presented in the inset to figure 5(a). As Ω grows, the oscillation frequency ν first increases, then reaches a plateau, and then decreases. It is worth noting (not shown in the figure) that ν weakly depends on other parameters such as $\sigma_{\rm i}$, $\sigma_{\rm d}$, δ and practically does not depend on Δ.

The oscillation spectra are shown in the inset plot to figure 5(b). The spectra clearly show the presence of 2nd and 3rd harmonics, which indicates nonlinearity of such oscillations. As the oscillations damp out,

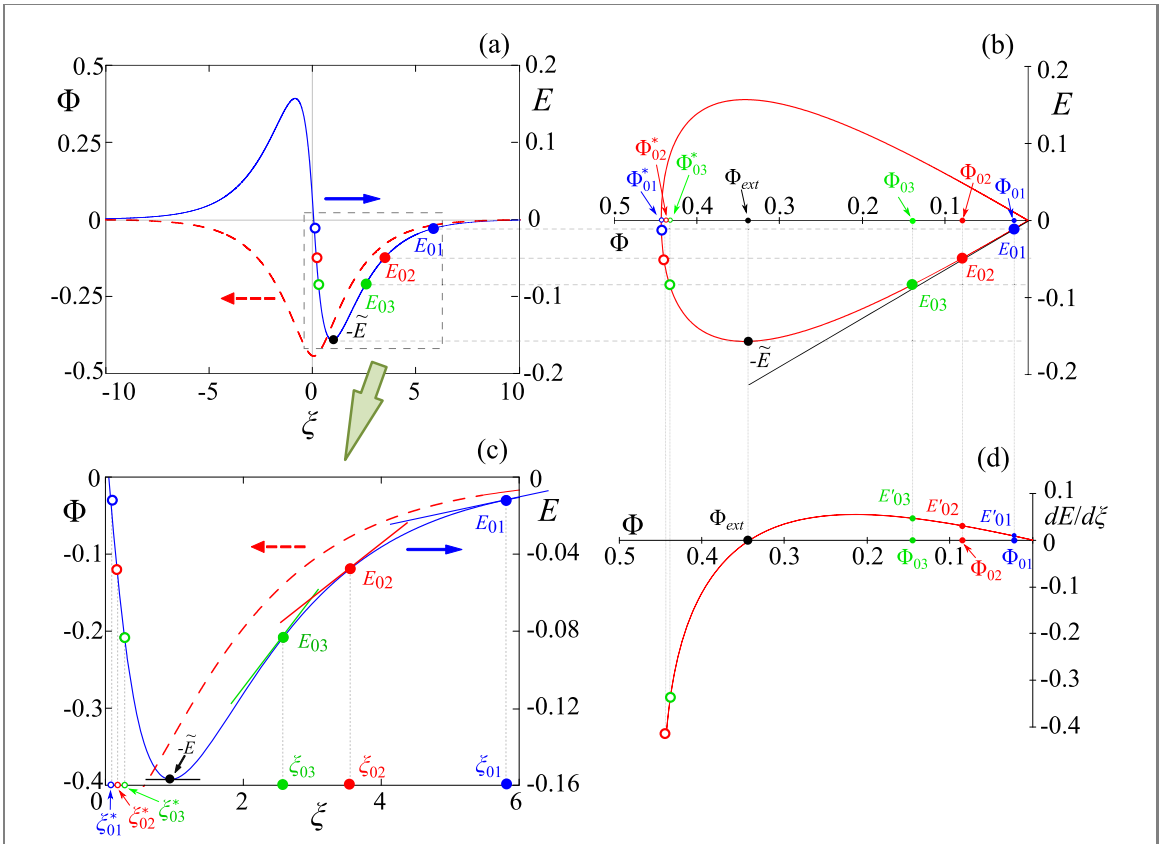

Figure 6. Relationship between oscillations parameters and soliton characteristics for different values of Ω. Parameters with subscripts '01', '02', '03' correspond to the values Ω = 0.01, Ω = 0.04, Ω = 0.07. (a),(c) Profiles of the soliton Φ(ξ) and $E(\xi)$ at $\sigma_i = 0.2$, $\sigma_d = 0.02$, $\delta = 10$, $M = 1.19$; (b) the phase portrait of a soliton, i.e. dependence $E(\Phi)$; (d) dependence $E'(\Phi)$, where $E' = dE/d\xi$.

the process linearizes, so that it can be described in a linear approximation (see section 3.2). The asymptotic positions of particles at $\tau \to \infty$ are denoted as ξ_{01}, ξ_{02}, ξ_{03} for Ω = 0.01, 0.04, and 0.07, respectively. These are equilibrium points for oscillating particles. As can be seen from figure 5(a), points ξ_{01}–ξ_{03} are placed inside the soliton at its leading front, and their position depends on Ω. In the wave frame, after relaxation of oscillations, the particle stops at the equilibrium point. In this case, we have $\xi = \xi_0$, $d\xi/d\tau = 0$, $d^2\xi/d\tau^2 = 0$. Then, from equation (13), we can obtain the equilibrium point condition:

$$-\frac{\partial \Phi}{\partial \xi} \equiv E = -\Omega M. \tag{16}$$

In the general case (for particles of arbitrary sign), equality (16) can be written as $|E| = \Omega M$. For the stationary confinement of trapped particles, equality (16) is sufficient, but for particle capture, electric field E must be greater than ΩM ($|E| > \Omega M$), because in this case it is necessary to reduce the initial velocity of the incident particle. On the other hand, if the condition $\tilde{E} < \Omega M$ is satisfied (where $\tilde{E}$ is the amplitude of the soliton electric field), the wave cannot retain dust particles. In this case, trapping is not possible. The soliton profiles and the $E(\Phi)$, $E'(\Phi)$ plots are shown in figure 6, where $E' = dE/d\xi$. Equilibrium points ξ_0 are marked on the plots. Figure 6 shows that all points ξ_0 are placed in the region of a positive gradient of the electric field. In this case, condition (16) is also satisfied for the points ξ'_0. However, such equilibrium is unstable, indeed, an infinitesimal fluctuation can shift a particle to the left where $|E| < \Omega M$. The condition for the field gradient then can be written as follows:

$$\frac{\partial E}{\partial \xi} > 0. \tag{17}$$

Now let us consider some properties of equilibrium points. Analytical expression for $\frac{\partial E}{\partial \xi}$ and $E(\Phi)$ are given by (9) and (12). The electric field corresponding to points $\xi = \xi_0$ is:

$$E_0 = -\Omega M. \tag{18}$$

Hereinafter, we consider the negative branch of function (12), which describes the leading edge of the soliton. Corresponding potential Φ_0 can be derived from equation (12):

$$E_0 + \sqrt{-2U(\Phi_0)} = 0. \tag{19}$$

We introduce the notation Φ_0 and $\Phi^*{}_0$ for the roots of equation (19). These roots are marked with '•' and '○' symbols in the phase portrait shown in figure 6(b). Roots Φ_0, which are closer to zero, satisfies condition (17). Equation (19) is an implicit function $\Phi(E)$ so we can obtain Φ_0 from this equation by using graphical or numerical methods. Knowing E_0 and Φ_0, we can calculate positions ξ_0, since functions $E(\xi)$ and $\Phi(\xi)$ are known (figure 6(a)). It is obvious that with increasing of Ω, the value of ξ_0 decreases ($\xi_{01} > \xi_{02} > \xi_{03}$). This means that equilibrium point ξ_0 moves to the center of the soliton as the value of the dissipation term is increase. Minimal possible value $\xi_0 = \xi_{0cr}$ corresponds to the amplitude $\tilde{E}$ of the soliton electric field as shown in figures 6(a) and (c). For $\xi_0 < \xi_{0cr}$, condition (17) is not satisfied. Therefore, for any given soliton, there is a limiting value of Ω_{cr}, such that for $\Omega > \Omega_{cr}$, the no-trough trapping is not possible. For the case shown in figure 6, $|\tilde{E}| = -0.157$ and, therefore, $\Omega_{cr} = \frac{\tilde{E}}{M} = 0.132$ in accordance with equation (18). Electric field amplitude $\tilde{E}$ can be found from (12) as an extremum of function $\tilde{E} = \sqrt{-2U(\Phi_{ext})}$, where Φ_{ext} is a root of the equation $\frac{\partial E}{\partial \Phi} = -\frac{\partial}{\partial \Phi}\sqrt{-2U(\Phi)} = 0$. The minus sign corresponds to the leading front of the soliton, where the electric field is negative. As a result we can write:

$$\frac{1}{\sqrt{-2U(\Phi)}}\frac{\partial}{\partial \Phi}U(\Phi) = 0.$$

Taking into account expression (12), as well as the fact that $\frac{\partial}{\partial \Phi}U(\Phi) = \delta_e \exp(\sigma_i \Phi) - \delta_i \exp(-\Phi) + N_d(\Phi)$ finally gives us:

$$\frac{\delta_e \exp(\sigma_i \Phi) - \delta_i \exp(-\Phi) + N_d(\Phi)}{E(\Phi)} = 0.$$

To satisfy this equality, it is enough that the numerator is equal to zero, so the final equation for Φ_{ext} takes the following form:

$$\delta_e \exp(\sigma_i \Phi_{ext}) - \delta_i \exp(-\Phi_{ext}) + N_d(\Phi_{ext}) = 0. \tag{20}$$

The value of Φ_{ext} can be found graphically or numerically, since equation (20) is transcendental. The positions of points E_0, ξ_0, Φ_0, $\tilde{E}$ are shown in figures 6(a)–(c). Figure 6(d) shows the function $E'(\Phi)$ and its root Φ_{ext}, according to equations (9) and (20). As mentioned above, the larger Ω, the closer ξ_0 is to the center of the soliton, and the smaller the possible amplitude of oscillations (figure 5), since the trapped particles should not fall into the rear edge of the soliton. Indeed, the electric field at the rear edge of the soliton becomes positive (see figures 2 and 6(a)), now it pushes the particle to the left so the particle becomes a transit one. We can conclude that the rear edge of the soliton does not affect the scattering or trapping process.

A more detailed analysis shows that the point of maximum displacement of trapped particles from their equilibrium positions is not at the center of the soliton, but at the point $\xi = \xi_0'$ (see section 2.3 in [34]). Thus, the maximum amplitude of the negative half-period of oscillations is $\tilde{\xi}_- = \xi_0 - \xi_0'$. Indeed, in the position of maximum deviation from equilibrium, the particle stops in order to reverse direction. At this point $v^*{}_d = 0$, therefore, the acceleration of the particle is easy to find from Newton's second law $a(\xi'_0) = -E_0 - \Omega M = 0$. Trapping is possible if the inequality $a > 0$ is satisfied (i.e. the particle moves towards the equilibrium point). This condition can be satisfied only to the right of the point ξ'_0 (at $\xi > \xi_0'$). Thus, the roots ξ'_0 can be used, firstly, to calculate the maximum amplitude of oscillations, secondly, to choose the initial conditions for equation (13).

The applied significance of formulas (16)–(20) includes the possibility of estimating the electric field magnitude of nonlinear waves if the no-trough trapping process was registered, and the value of Ω is known. On the other hand, if parameters of a soliton are given, then Ω can be calculated. Formulas (16)–(20) also allow one to estimate parametric regions in which the no-trough trapping of particles and the oscillatory process occurs. This is a subject for future works.

3.2. A new oscillatory process. Linear approximation

As shown in figure 5, as the oscillation amplitude decreases, the process linearization is observed. In this section we discuss a linear approximation for the oscillatory process.

Let us consider the wave frame case. A particle position $\xi(\tau)$ can be expressed as $\xi = \tilde{\xi} \exp[i(\omega_0 - i\gamma)\tau]$, where $\tilde{\xi}$ is the initial amplitude, ω_0 is natural frequency of the oscillations, γ is decrement. We assume that oscillations occur around equilibrium position ξ_0 with a small amplitude. The Taylor series

expansion of the electric field function gives:

$$\begin{array}{c} E(\xi) = E(\xi_0) + E'(\xi_0)(\xi - \xi_0) \\ \text{or} \\ E(\xi) = E'(\xi_0)\,\xi + A \end{array}, \tag{21}$$

where $E(\xi_0) = E_0$, $E'(\xi_0) = E'_0$. The constant A is given by expression $A = E_0 - E'_0\xi_0$. It is obvious that $E'_0 = E'(\Phi_0)$. In turn, the dependence $E'(\Phi)$ is described explicitly by equation (9) and is displayed in figure 6(d). As shown above, the value of Φ_0 can be determined from equation (19) numerically or graphically. It is easy to see that expression (21) describes the tangents to the electric field profile at $\xi = \xi_0$, as it is shown in figure 6(b). Now, taking into account that $\frac{d\Phi}{d\xi} = -E$, we substitute equation (21) in (13):

$$\frac{d^2\xi}{d\tau^2} = -\Omega\frac{\partial\xi}{\partial\tau} - E'_0\xi + B, \tag{22}$$

where $B = -\Omega M - A$, taking into account formula (18) we have $B = E'_0\xi_0$. Equation (22) describes a linear damped harmonic oscillator. For the weak dissipation case, if inequality $\Omega < 2\sqrt{E'_0}$ holds, the solution of equation (22) is given by the following formula:

$$\begin{array}{l} \xi(\tau) = \tilde{\xi}\,\exp(-\gamma\tau)\sin[\omega\tau + \varphi] + \xi_0 \\ \text{or} \\ \xi(\tau) = \tilde{\xi}\,\exp[\mathrm{i}(\omega + \mathrm{i}\gamma)\tau] + \xi_0, \end{array} \tag{23}$$

where

$$\omega = \sqrt{E'_0 - \frac{\Omega^2}{4}}, \qquad \gamma = \frac{\Omega}{2}. \tag{24}$$

From (24) follows that the frequency and decrement depend only on Ω and E'_0. The first parameter is given, the second can be obtained from equations (9), (12) and (18) as follows. From equation (18) we get E_0. Next, we substitute the obtained value into equation (12) and find Φ_0. In accordance with condition (17), the root closest to zero should be used (see figure 6(b)). Finally, from equation (9) we determine $E'_0 = E'(\Phi_0)$. It is important to note that to calculate E'_0 (and hence ω) there is no need to obtain the soliton profile function, which requires numerical computations. The soliton profile function is necessary only in order to obtain ξ_0.

The weak side in the linear analysis of new oscillations is equation (12), the explicit solutions of which are not known. However, as one can see from figure 6(b), the roots of this equation placed in the area close to a straight line. Therefore, to get an approximate analytical solutions, one can use the Taylor series expansion for the right-hand side of equation (12).

$$E(\Phi) = \sqrt{2}\sqrt{\frac{\delta + \sigma_\mathrm{i}}{\delta - 1} - \frac{1}{M^2 - 3\sigma_\mathrm{d}}}\Phi \tag{25}$$

The approximation (25) is shown as a thin straight line in figure 6(b). As one can see, the linear approximation is quite accurate for the roots ξ_{01}–ξ_{03}. Now, the oscillation frequency can be expressed explicitly:

$$\omega(\Phi_0, M, \delta, \sigma_\mathrm{i}, \sigma_\mathrm{d}, \Omega) = \sqrt{\delta_\mathrm{e}\,\exp(\sigma_\mathrm{i}\Phi_0) - \delta_\mathrm{i}\,\exp(-\Phi_0) + N_\mathrm{d}(\Phi_0, M, \delta, \sigma_\mathrm{i}, \sigma_\mathrm{d}) - \Omega^2/4}$$

with

$$\Phi_0 = -\frac{\Omega M}{\sqrt{\frac{\delta+\sigma_\mathrm{i}}{\delta-1} - \frac{1}{M^2-3\sigma_\mathrm{d}}}}. \tag{26}$$

Here $N_\mathrm{d}(\Phi_0, M, \delta, \sigma_\mathrm{i}, \sigma_\mathrm{d})$ is determined by equation (10). The dependences $\nu(\Omega)$, $\omega(\Omega)$ (where $\nu \equiv \omega/2\pi$), calculated by formula (26) are shown by solid curves in the inset to figure 5(a) for different values of M (i.e. for different soliton amplitudes). Also, for comparison, the exact dependences $\nu(\Omega)$, are presented, calculated using the oscillation spectra (symbols '▲' and 'Δ' for $M = 1.19$ and $M = 1.05$, respectively). As one can see, the numerical result is in a good agreement with the approximate analytical approach, especially for small values of Ω. Even more accurate seems the quadratic approximation of the function $E(\Phi)$, which can be expressed by rather complicated formulas. Detailed analysis of the quadratic approximation is beyond the scope of this work.

As can be seen from the inset to figure 5(a), the oscillation frequency ν first increases with increasing Ω, then reaches a plateau, and then decreases. This behavior of the function $\nu(\Omega)$ is explained as follows. Equation (24) implies $\nu = \frac{\omega}{2\pi} \approx \frac{\sqrt{E_0'}}{2\pi}$. Thus, the oscillation frequency ν depends on the derivative $\frac{dE}{d\xi}|_{\xi=\xi_0}$, i.e. on the angle of inclination of the tangent to the graph $E(\xi)$ (see figures 6(a) and (c)). With the growth of Ω, the equilibrium point moves from right to left ($E_{01} \to E_{02} \to E_{03} \to -\tilde{E}$). In this case, the angle of inclination of the tangent increases at $E_{01} \to E_{02} \to E_{03}$. However, as we approach point $\tilde{E}$ ($E_0 \to \tilde{E}$), the tilt angle will pass its maximum and begin to decrease, reaching zero at point $\tilde{E}$.

The main characteristic of an oscillatory process is frequency. As can be seen from the inset to figure 5(a), the frequencies of the oscillations under consideration are less than ω_d. Moreover, $\omega \ll \omega_d$ at small values of the parameter Ω. Thus, the new oscillatory process is low-frequency.

The process under study is oscillatory, since it describes the motion of separate (independent) particles. Analyzing a coupled ensemble of such particles, one should expect the appearance of wave properties, we leave it as a topic for future works.

4. Comparison with experiments and discussion

In experimental work [19] the breaking process of a nonlinear supercritical electron wave in a collisionless plasma with microwave excitation was studied. The wave intensity was 10^4 times higher than the breaking threshold intensity. Generation of accelerated electrons was observed, their velocity was twice the phase velocity of the wave. An electron plasma wave is a wave packet and it is not an exact analogue to acoustic solitons. Electron motion in the electric field of such wave is oscillatory. Nevertheless, for larger amplitudes it was found that multi-streaming flow occurs in on the first oscillation [17]. For strongly nonlinear electron waves, the steepness of the envelope is large, hence the amplitude of the plasma oscillations increases rapidly (see figure 1 from [19]). Therefore, in the first approximation, the influence of previous oscillations can be neglected when calculating the parameters of reflected particles. Thus, in our opinion, experiment [19] can be considered an example of elastic scattering of charged particles by a wave in the non-dissipative environment.

Let us consider further examples of inelastic scattering of particles by a soliton-like potential. In [16], the breaking of the self-excited DA soliton of supercritical amplitude in a collisional dusty plasma of a glow discharge was studied. Taking into account our normalizations, the main parameters of the plasma are $\delta = 3$, $\sigma_i = 0.17$, $M = 1.2$, $\Omega = 0.07$. The acceleration of charged dust particles by the leading edge of a supercritical soliton was observed. It was shown that the speed of the accelerated particles is approximately equal to the speed of the soliton, which corresponds to inelastic scattering. In [16], for the first time, the considered oscillations of particles were discovered. Only the first half-period of oscillations was observed, the duration of which was well described by the constructed theoretical model. Our model makes it possible to estimate the wave electric field in the region where the trapped particles are presented ($z \gtrsim 4$ mm in figure 2 from [16]). Equation (18) gives $E_0 \approx 6$ V cm^{-1} for the parameters and normalization given in [16].

The evolution of plane DA waves and the no-trough trapping of dust particles in collisional rf dusty plasma were studied in [14, 15]. The discharge parameters correspond in order of magnitude to those from [16]. The wave evolution consisted of the following stages:

(a) Excitation in the upper part of the cloud;
(b) Linear gain;
(c) Nonlinear steeping;
(d) Breaking, which occurs along with the trapping of particles and the kinetic heating of the dust fraction;
(e) Stationary propagation of the nonlinear wave with trapped particles;
(f) Decay of the wave at the bottom of the dust cloud.

The observed wave at the end of the third stage of evolution, before breaking, acquired a strongly nonlinear soliton-like profile (figure 1(c) in [14], bold curve, at $z = 0$). The wave reached its supercritical amplitude at the breaking point, which led to the acceleration of particles to velocity approximately equal to the velocity of the wave, and the subsequent trapping of dust particles. It is interesting to note that after the breaking the wave did not decay, but continued to move in the same direction with the same velocity. After breaking, a change in the amplitude and width of the dust density profiles was observed. The same experiment was considered in work [15]. The kinetic temperature of the dust component after breaking was estimated, which gave the value $T_d = 60$ eV or $\sigma_d = 0.24$. Before the breaking, T_d was much smaller. This difference in temperature can explain the broadening of the wave profile upon passing the critical point. Particles trapped during the breaking continued to move along with the wave, forming a rather extended cloud, localized in the region of the leading edge of the wave (see figure 4 from [15]). The length of this

cloud is apparently determined by the Coulomb repulsion and various fluctuations. Figure 4 from [15] shows the 'ragged' dust density profile of the wave that contains trapped particles. This fact may indicate a possible phase grouping of trapped particles and a possible dispersion of the new wave mode. In this respect, the experiment presented in [35] seems to be interesting. This paper describes secondary DA waves observed in the vicinity of primary large amplitude nonlinear self-exited DA waves. The experiment was carried out in a dc glow discharge plasma in argon at a pressure of 24 Pa. According to the authors of [35], the cause of secondary waves is streaming instability. Unfortunately, data on the motion of individual particles were not presented in [35]. Therefore, at this stage, we cannot perform a detailed analysis of the experiment [35]. However, such an analysis is possible in the future, after generalizing our theory to an ensemble of coupled charged particles.

The new plasma oscillatory process can play an important role in various parametric resonances and manifest itself in broadening of the pump wave spectrum. Waves containing trapped particles can be periodic [14, 15], which increases the efficiency of possible parametric processes. On the other hand, one can parametrically 'heat up' trapped particles by choosing the frequency of the pump. The oscillation phases of different particles in our model are random. In self-consistent models, phase grouping is possible. On the other hand, coherent oscillatory motion of particles can be realized with parametric excitation of oscillations. Indeed, in this case, the driving force in the first approximation will be harmonic for all trapped particles. Thus, one should expect the in-phase motion of all such particles.

Experiments [14, 15] demonstrate the stability of waves containing 'no-trough' trapped particles, which confirms the practical significance of our findings. Obtained results can be easily generalized to ion- and electron-acoustic models, as well as to more complex dust-acoustic models, including non-thermal electrons (ions), self-consistent dust charge, etc. An important condition for the existence of such modes is the presence of dissipation. It is worth mentioning that the presence of dissipation is a necessary condition for the existence of another type of instability, called resistive instabilities [36].

5. Conclusions

The process of reflection (scattering) of charged particles by the leading edge of a DA soliton is described theoretically. It is shown that the scattering is elastic in the collisionless (conservative) case and inelastic in the presence of dissipation. In the first case, the velocity of reflected particles is close to twice the wave velocity, which has been observed in experiments [19]. In the second case, the velocity of reflected particles is approximately equal to the velocity of the wave; the particles seem to 'stick' to the leading edge of the soliton or a nonlinear wave. This type of scattering was observed in experiments [14–16]. In the second case, the motion of charged particles can be oscillatory. The analysis of these oscillations is carried out. Spectra, decrements and other parameters are calculated. In particular, it is found that the oscillatory process is low-frequency: $\omega \ll \omega_d$. The applied significance of the results obtained is briefly considered.

Data availability statement

All data that support the findings of this study are included within the article (and any supplementary files).

ORCID iDs

F M Trukhachev https://orcid.org/0000-0002-9099-615X
N V Gerasimenko https://orcid.org/0000-0002-4118-6142
M M Vasiliev https://orcid.org/0000-0002-0425-1152

References

[1] Adam J 1987 *Plasma Phys. Control. Fusion* **29** 443
[2] Modena A *et al* 1995 *Nature* **377** 606
[3] Adli E *et al* 2018 *Nature* **561** 363
[4] Ginzburg V L 1979 *Theoretical Physics and Astrophysics* (Amsterdam: Elsevier) p 457
[5] Landau L D 1946 *J. Phys. USSR* **10** 25
[6] Alexandrov A F, Bogdankevich L S and Rukhadze A A 1984 *Principles of Plasma Electrodynamics* ed A A Rukhadze (Berlin: Springer) p 490
[7] Molotkov V I *et al* 1999 *JETP* **89** 447
[8] Kruer W L, Dawson J M and Sudan R N 1969 *Phys. Rev. Lett.* **23** 838
[9] Bernstein I B, Greene J M and Kruskal M D 1957 *Phys. Rev.* **108** 546
[10] Friedland L, Khain P and Shagalov A G 2006 *Phys. Rev. Lett.* **96** 225001

[11] Trukhachev F M and Tomov A V 2016 *Cosmic Res.* **54** 351
[12] Trukhachev F M, Tomov A V, Mogilevsky M M and Chugunin D V 2018 *Tech. Phys. Lett.* **44** 494
[13] Trukhachev F M, Vasiliev M M and Petrov O F 2020 *High Temp.* **58** 520–38
[14] Teng L-W, Chang M-C, Tseng Y-P and Lin I 2009 *Phys. Rev. Lett.* **103** 245005
[15] Chang M C, Teng L W and Lin I 2012 *Phys. Rev. Lett.* **85** 046410
[16] Trukhachev F M, Vasiliev M M, Petrov O F and Vasilieva E V 2019 *Phys. Rev.* E **100** 063202
[17] Dawson J M 1959 *Phys. Rev.* **113** 383
[18] CofTey T P 1971 *Phys. Fluids* **14** 1402
[19] Bauer B S, Wong A Y, Decyk V K and Rosenthal G 1992 *Phys. Rev. Lett.* **68** 3706
[20] Flanagan T M and Goree J 2010 *Phys. Plasmas* **17** 123702
[21] Flanagan T M and Goree J 2011 *Phys. Plasmas* **18** 013705
[22] Petrov O F, Trukhachev F M, Vasiliev M M and Gerasimenko N V 2018 *J. Exp. Theor. Phys.* **126** 842
[23] Schwabe M, Rubin-Zuzic M, Zhdanov S, Thomas H M and Morfill G E 2007 *Phys. Rev. Lett.* **99** 095002
[24] Trukhachev F M, Vasiliev M M, Petrov O F and Vasilieva E V 2021 *J. Phys. A: Math. Theor.* **54** 095702
[25] Heinrich J, Kim S-H and Merlino R L 2009 *Phys. Rev. Lett.* **103** 115002
[26] Akhmediev N and Ankiewicz A 2005 *Dissipative Solitons* (*Lecture Notes in Physics* vol 661) (Berlin: Springer)
[27] Fortov V E *et al* 2004 *Phys.-Usp.* **47** 447
[28] Fortov V E *et al* 2000 *Phys. Plasmas* **7** 1374
[29] Ghosh S, Adak A and Khan M 2014 *Phys. Plasmas* **21** 012303
[30] Khan S, Rahman A, Hadi F, Zeb A and Khan M Z 2017 *Contrib. Plasma Phys.* **57** 223
[31] Mendoza-Briceno C A, Russel S M and Mamun A A 2000 *Planet. Space Sci.* **48** 599
[32] Shukla P K and Mamun A A 2002 *Introduction to Dusty Plasma Physics* (Bristol: Institute of Physics Publishing)
[33] Merlino R L and D'Angelo N 2005 *Phys. Plasmas* **12** 054504
[34] Supplementary material (https://stacks.iop.org/NJP/23/093016/mmedia). Animation of solutions to equations (13) and (14), which describe the dynamics of the wave–particle interaction.
[35] Heinrich J R, Kim S-H, Meyer J K, Merlino R L and Rosenberg M 2012 *Phys. Plasmas* **19** 083702
[36] Shivamoggi B K 1985 *Astrophys. Space Sci.* **114** 15